$LaBr_3$:Ce and SiPMs for time-of-flight PET: achieving 100 ps coincidence resolving time

2010 Phys. Med. Biol. 55 N179

(http://iopscience.iop.org/0031-9155/55/7/N02)

Phys. Med. Biol. **55** (2010) N179–N189 doi:10.1088/0031-9155/55/7/N02

NOTE

$LaBr_3$:Ce and SiPMs for time-of-flight PET: achieving 100 ps coincidence resolving time

Dennis R Schaart[1], Stefan Seifert[1], Ruud Vinke[2], Herman T van Dam[1], Peter Dendooven[2], Herbert Löhner[2] and Freek J Beekman[1,3]

[1] Delft University of Technology, Radiation Detection & Medical Imaging, Mekelweg 15, 2629 JB Delft, The Netherlands
[2] Kernfysisch Versneller Instituut, University of Groningen, Zernikelaan 25, 9747 AA, Groningen, The Netherlands
[3] Rudolf Magnus Institute of Neurosciences and Image Sciences Institute, University Medical Centre Utrecht, Heidelberglaan 100, 3584 CG, Utrecht, The Netherlands

E-mail: d.r.schaart@tudelft.nl

Received 1 October 2009, in final form 14 January 2010
Published 19 March 2010
Online at stacks.iop.org/PMB/55/N179

Abstract

The use of time-of-flight (TOF) information in positron emission tomography (PET) enables significant improvement in image noise properties and, therefore, lesion detection. Silicon photomultipliers (SiPMs) are solid-state photosensors that have several advantages over photomultiplier tubes (PMTs). SiPMs are small, essentially transparent to 511 keV gamma rays and insensitive to magnetic fields. This enables novel detector designs aimed at e.g. compactness, high resolution, depth-of-interaction (DOI) correction and MRI compatibility. The goal of the present work is to study the timing performance of SiPMs in combination with $LaBr_3$:Ce(5%), a relatively new scintillator with promising characteristics for TOF-PET. Measurements were performed with two, bare, 3 mm × 3 mm × 5 mm $LaBr_3$:Ce(5%) crystals, each coupled to a 3 mm × 3 mm SiPM. Using a ^{22}Na point source placed at various positions in between the two detectors, a coincidence resolving time (CRT) of ∼100 ps FWHM for 511 keV annihilation photon pairs was achieved, corresponding to a TOF positioning resolution of ∼15 mm FWHM. At the same time, pulse height spectra with well-resolved full-energy peaks were obtained. To our knowledge this is the best CRT reported for SiPM-based scintillation detectors to date. It is concluded that SiPM-based scintillation detectors can provide timing resolutions at least as good as detectors based on PMTs.

(Some figures in this article are in colour only in the electronic version)

1. Introduction

The use of time-of-flight (TOF) information in positron emission tomography (PET) has recently been demonstrated to enable significant improvement in image noise properties and, therefore, lesion detection, especially in heavier patients (Kadrmas *et al* 2009, Lois *et al* 2010, Moses 2007, Muehllehner and Karp 2006, Surti *et al* 2007). This warrants further research into TOF-capable PET scintillation detectors, in particular with the aim to obtain better timing resolution.

The relatively new inorganic scintillator $LaBr_3$:Ce has high potential for TOF-PET (Kuhn *et al* 2006). Commercial-grade $LaBr_3$:Ce(5%) has a fast decay time of ∼16 ns (Bizarri and Dorenbos 2007), a high light yield of ∼70.000 photons MeV^{-1} (de Haas and Dorenbos 2008), an excellent energy resolution of ∼2.6% FWHM at 662 keV (Drozdowski *et al* 2007), a mass density of 5.1 g cm^{-3} (Higgins *et al* 2006) and an effective atomic number of 46.9 (van Eijk 2002). To optimally benefit from the advantages of $LaBr_3$:Ce in a PET detector, the scintillation light should be read out using a photosensor with fast response and high photodetection efficiency (PDE) at the $LaBr_3$:Ce emission wavelengths (∼380 nm).

Excellent coincidence resolving times (CRTs) have already been demonstrated with $LaBr_3$:Ce crystals of various dimensions and Ce concentrations, coupled to fast photomultiplier tubes (PMTs) (Kuhn *et al* 2005, Kyba *et al* 2008, Glodo *et al* 2006). However, silicon photomultipliers (SiPMs) are turning into a promising alternative for PMTs, as of recently (Antich *et al* 1997, Bondarenko *et al* 2000, Britvitch *et al* 2007, Golovin and Saveliev 2004, Herbert *et al* 2007, Lewellen 2008, McElroy *et al* 2007, Musienko *et al* 2007, Renker 2007, Yamamoto *et al* 2007). Similar to PMTs, SiPMs have a gain in the order of $\sim 10^6$. In addition, these solid-state devices are much more compact and essentially transparent to 511 keV gamma rays. This enables novel detector designs aimed at, for example, compactness, high resolution, depth-of-interaction (DOI) correction, etc (España *et al* 2010, Kolb *et al* 2008, Llosá *et al* 2008, Nishikido *et al* 2008, Pestotnik *et al* 2008, Schaart *et al* 2008b, 2009, Song *et al* 2008). Moreover, in contrast with PMTs, SiPMs are compatible with magnetic fields, a feature that is very interesting in light of recent endeavours to combine PET and MRI into hybrid imaging devices (Catana *et al* 2006, Judenhofer *et al* 2008, Shao *et al* 1997, Townsend 2008).

The goal of the present work is to study the timing performance of commercially available 3 mm × 3 mm SiPMs in combination with $LaBr_3$:Ce(5%) for TOF-PET. We use relatively small $LaBr_3$:Ce(5%) crystals to minimize time walk due to the variation of photon path lengths with the position-of-interaction. However, when using larger crystals, one may attempt to achieve similarly good timing resolution by applying a position-of-interaction correction to the timing information (Moses and Derenzo 1999, Shibuya *et al* 2008, Vinke *et al* 2008).

2. Materials and methods

2.1. Detectors

Measurements were performed with two, identical, SiPM-based scintillation detectors. In each detector a bare 3 mm × 3 mm × 5 mm $LaBr_3$:Ce(5%) crystal (Saint-Gobain BrilLanCe 380) was enclosed in a reflective casing made from Spectralon, a PTFE-based material with reflectivity specified to be better than 98% at 380 nm, i.e. the wavelength of maximum emission of $LaBr_3$:Ce(5%). A 3 mm × 3 mm SiPM (Hamamatsu MPPC-S10362-33-050C) was coupled directly to each of the $LaBr_3$:Ce crystals using a transparent silicone encapsulation gel (Lightspan LS-3252). Each SiPM consists of an array of 3600 self-quenched Geiger Mode

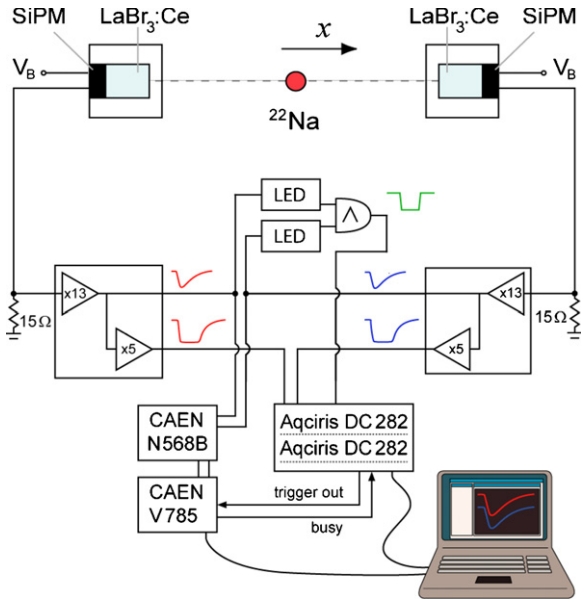

Figure 1. Schematic overview of the experimental setup. See the text for explanation.

Avalanche Photodiodes at a pitch of 50 μm. Both SiPMs were operated at ~2.0 V above their breakdown voltages, which were measured to be ~69.7 V and ~70.1 V, respectively. All experiments were performed at room temperature and in a dry atmosphere to protect the hygroscopic LaBr$_3$:Ce crystals.

2.2. Measurement setup

Figure 1 shows a schematic representation of the measurement setup. The two detectors and a ^{22}Na point source (Isotope Products Laboratories, active volume ∅ 0.5 mm × 1 mm) were mounted on an optical rail, such that the source could be placed at various positions x in between the two detectors.

The SiPM charge pulses were converted to voltage pulses by means of 15 Ω shunt resistors and fed into voltage preamplifiers made in-house. Each preamplifier consisted of two cascaded amplification stages, as indicated in figure 1. The first amplification stage (gain ~13) consisted of a Texas Instruments OPA847 opamp in a non-inverting configuration with a feedback resistor of 270 Ω and a 22 Ω resistor to ground. The second stage (gain ~5) consisted of an ac-coupled monolithic microwave integrated circuit (MMIC) low noise amplifier (Avago Technologies MGA-61563). Care was taken to minimize the total length of the leads between the SiPM and the preamplifier (<1 cm).

In the timing experiments, the signals of the first amplification stages were used to obtain a coincidence trigger, by feeding them into LeCroy 825 leading edge discriminators (LEDs) and connecting the discriminator outputs to a LeCroy 465 coincidence unit. The signals of the first amplification stages were also used to determine the two pulse heights of each coincident pulse pair. This was done by feeding these signals into a CAEN N568B multi-channel shaping amplifier (shaping time 100 ns) connected to a CAEN V785 multi-channel, peak-sensitive ADC.

The pulses from the secondary amplification stages of the two preamplifiers were digitized by two, synchronized, Acqiris DC282 fast sampling ADCs. Both ADCs were operated at the maximum sampling rate of 8 GS s^{-1} and at a 10-bit resolution. The synchronization clock jitter between the two ADCs is specified to be $\leqslant$1 ps. The trigger for the two synchronized ADCs was provided by the above-mentioned LeCroy 465 coincidence unit. The gain of the secondary amplification stages was chosen such that the ADC input range (set to 500 mV) corresponded to only ∼12.5% of the amplitude of a 511 keV pulse. As the optimum trigger threshold for timing lies within this portion of the pulse rising edge, this approach minimizes the contribution of ADC noise to the overall signal-to-noise ratio of the digitized (partial) pulse traces. The traces of each coincident pulse pair were stored in a PC, together with the corresponding pulse heights recorded by the CAEN V785 ADC. The stored data were subsequently used for offline, digital time pick-off as described in section 2.3.

Experiments were also performed by irradiating the detectors with a ^{22}Na source and feeding the signals from the first amplification stages of the preamplifiers directly into the Acqiris ADCs, using an ADC input range larger than the maximum pulse amplitude and applying no coincidence condition. About 10^5 full pulse traces thus acquired were stored for offline analysis of the pulse shape and energy content.

2.3. Digital time pickoff

A selection of digitized pulse traces for timing analysis was performed using the pulse height information recorded by the CAEN V785 ADCs. Only events with energies between ∼490 keV and ∼532 keV were accepted, corresponding to the full-width-at-tenth-maximum (FWTM) of the full-energy peak. Time stamps were subsequently derived by interpolating each trace with a cubic spline and determining the intersection of the interpolated data with a fixed threshold relative to the baseline, set at approximately nine times the pulse height of a single photon pulse. The baseline was determined for each trace individually as the average signal in the region between ∼1.2 ns and ∼0.2 ns before the onset of the pulse.

3. Results

3.1. Pulse shape

Figure 2 shows some typical examples of 511 keV pulse traces from the two detectors. These were obtained by feeding the outputs of the first amplification stages of the preamplifiers directly into the Acqiris DC282 ADCs. The average 10–90% rise time of the pulses in the full-energy peak equals ∼9 ns. As the pulse shape equals the convolution of the scintillation light pulse and the SiPM response, the rise time is primarily determined by the low pass (i.e. integrating) characteristics of the SiPM and the scintillation decay time. The influence of the high-bandwidth preamplifiers and other electronics on the pulse rise time is expected to be negligible in our measurements.

3.2. Timing spectra

Figure 3 shows the timing spectra obtained with the ^{22}Na point source located at positions $x_1 = -20$ mm $\pm$ 0.25 mm (green diamonds), $x_2 = 0$ mm $\pm$ 0.25 mm (black squares) and $x_3 = 20$ mm $\pm$ 0.25 mm (blue circles). These spectra were obtained using the digital time pickoff method described in section 2.3, using 3624, 7326 and 3346 coincident events per spectrum, respectively. The FWHM coincidence resolving times (CRTs), determined from Gaussian fits to the data (the red curves in the figure), are 101.8 ps, 99.5 ps and 103.4 ps for x_1,

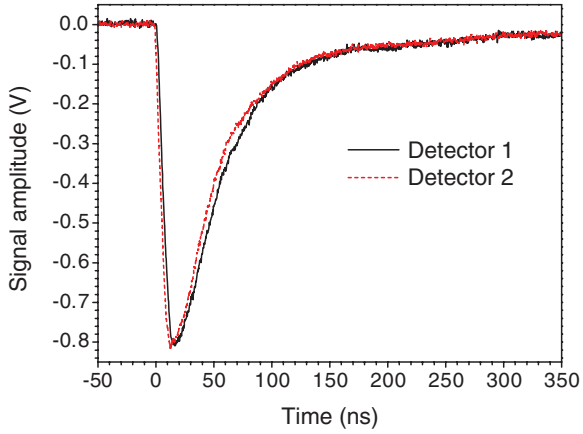

Figure 2. Typical digitized pulse traces of the two detectors, measured with 511 keV photons. The average 10–90% rise time of the recorded 511 keV pulses equals ∼9 ns.

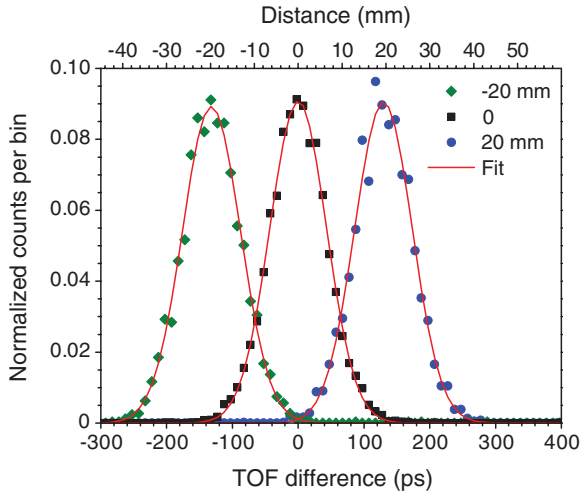

Figure 3. Timing spectra recorded with two 3 mm × 3 mm × 5 mm LaBr$_3$:Ce crystals read out by 3 mm × 3 mm SiPMs, using a ^{22}Na point source located at $x_1 = -20$ mm ± 0.25 mm (green diamonds), $x_2 = 0$ mm ± 0.25 mm (black squares), and $x_3 = 20$ mm ± 0.25 mm (blue circles). The red curves indicate Gaussian fits to the data. The average coincidence resolving time (CRT) equals 101 ps ± 2 ps FWHM, corresponding to 15.1 mm ± 0.3 mm FWHM.

x_2 and x_3, respectively. The weighted average of these values equals 101 ps ± 2 ps FWHM, corresponding to a TOF positioning resolution of 15.1 mm ± 0.3 mm FWHM.

3.3. Pulse height spectra

Figure 4 shows the ^{22}Na pulse height spectra measured with both detectors. These were derived by integration of the digitized pulses from the first amplification stages of the preamplifiers. A baseline correction was applied to each pulse before integration. The 511 keV full-energy

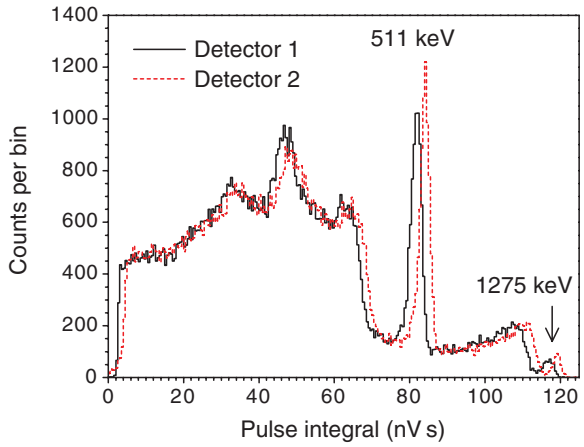

Figure 4. Pulse height spectra of the two detectors, measured using a ^{22}Na source. The observed widths of the 511 keV peaks are ∼3.7% FWHM and ∼3.2% FWHM for detector 1 and detector 2, respectively.

peaks can be seen to be superimposed on the Compton ridges of the 1275 keV peaks. The latter peaks are relatively small due to the small crystal size.

The observed widths of the 511 keV peaks are ∼3.7% FWHM and ∼3.2% FWHM for detector 1 and detector 2, respectively. These small widths are partly due to SiPM saturation, as discussed in more detail in section 4.3. Nevertheless, all full-energy peaks are well resolved and can be clearly distinguished from the corresponding Compton ridges.

4. Discussion

4.1. Timing performance

The above results were achieved using detectors based on 3 mm × 3 mm × 5 mm $LaBr_3$:Ce(5%) crystals and 3 mm × 3 mm SiPMs. To obtain sufficient system sensitivity, a clinical TOF-PET scanner might, for example, be based on several stacked layers of such detector elements. Alternatively, the detector design might be based on longer crystals. The use of monolithic crystals read out by position-sensitive SiPM arrays may also be considered. While many different detector designs could thus be envisaged, the timing performance is generally expected to deteriorate in larger crystals due to the variation of photon path lengths with the position-of-interaction. Fortunately, it may be possible to at least partly correct for this effect if the position-of-interaction in the crystal is known (Moses and Derenzo 1999, Shibuya *et al* 2008, Vinke *et al* 2008). The results presented here may thus be seen as representing the CRT in principle achievable with $LaBr_3$:Ce(5%) and 3 mm × 3 mm SiPMs commercially available at the time of writing.

The present work can be compared to results obtained with SiPMs by other authors. Several studies have been performed using LSO:Ce and similar materials. Some of the best results reported are those from Göttlich *et al* (2008), which reached a CRT of 460 ps FWHM using two 3 mm × 3 mm × 15 mm lutetium fine silicate (LFS) crystals coupled to the same Hamamatsu SiPMs as the ones used here, those from Burr and Wang (2007), which obtained a CRT of 268 ps FWHM using two 3 mm × 3 mm × 10 mm LYSO:Ce crystals and prototypes of

the same SiPMs as used in the present study and those from Kim *et al* (2009), which achieved a CRT of 240 ps FWHM using 3 mm × 3 mm × 10 mm LYSO:Ce crystals coupled to the same SiPMs as those used here.

Few studies have so far been performed with $LaBr_3$:Ce (Schaart *et al* 2008a), presumably because of the difficulties encountered in using this hygroscopic material. To our knowledge the CRT obtained with $LaBr_3$:Ce(5%) in the present work is significantly better than those reported for LSO:Ce, LYSO:Ce and LFS to date.

It is acknowledged that the performance of a PET scintillator is not only determined by its timing resolution. Compared to LSO:Ce and similar materials, a disadvantage of $LaBr_3$:Ce is its lower stopping power, giving rise to increased intra- and inter-crystal scattering and requiring thicker detectors to obtain equal detection efficiency. In principle, thicker detectors may give rise to increased parallax errors. However, these can be mitigated by using stacked layers of small detector elements as mentioned above or by implementing some form of depth-of-interaction (DOI) correction, see e.g. Lewellen (2008) and references therein.

An important advantage of $LaBr_3$:Ce is its much higher light yield, which is a crucial factor for obtaining high spatial resolution. Moreover, both its superior timing (randoms suppression, TOF) and its excellent energy resolution (scatter rejection) are of great advantage to improve image quality, especially in heavier patients (Daube-Witherspoon *et al* 2010).

Given the above advantages and disadvantages, at present it is difficult to predict the overall performance of $LaBr_3$:Ce in comparison to other PET scintillators, especially since the only $LaBr_3$:Ce-based prototype scanner realized to date (Daube-Witherspoon *et al* 2010) has not yet been optimized with respect to all of the above factors. In contrast, LSO:Ce and similar materials are used in many commercial systems, most of which have undergone multiple iterations of optimization. Thus, further research into the use of $LaBr_3$:Ce in TOF-PET is warranted.

4.2. SiPMs versus PMTs

The average 10–90% rise time of ∼9 ns obtained in this study is relatively large compared to the values typically found with fast PMTs. For example, Kuhn *et al* (2005) measured a 10–90% rise time of ∼3 ns for a 4 mm × 4 mm × 30 mm $LaBr_3$:Ce(5%) crystal on a Hamamatsu R4998 PMT. In principle, a longer rise time is undesirable as the timing resolution σ_t associated with electronic and sampling noise is equal to the ratio of the noise and the signal slope (Wilmshurst 1985):

$$\sigma_t \sim \frac{\sigma_v}{dv/dt}, \tag{1}$$

where σ_v is the RMS noise voltage and dv/dt denotes the slope of the pulse leading edge at the point where it crosses the trigger level.

However, the absolute slope dv/dt is proportional to the photosensor photodetection efficiency. It is not trivial to specify the PDE of the SiPMs used here, since it is a function of bias voltage, temperature, degree of saturation, etc and varies between individual devices of the same type. However, according to the manufacturer's data sheet (Hamamatsu 2009), it may be as high as ∼45% at 380 nm, the wavelength of maximum emission of $LaBr_3$:Ce(5%). While it is to be noted that this figure includes contributions from cross-talk and after-pulsing (Du and Retière 2008, Yamamoto *et al* 2007), it is considerably higher than the quantum efficiency (QE) of, for example, the above-mentioned R4998 PMT, which is estimated to be ∼16% at 380 nm from the manufacturer's datasheet (Hamamatsu 1999). A second advantage of a higher PDE is that a larger number of primary charge carriers per pulse reduce the influence of statistical fluctuations on the timing resolution.

A full analysis of the timing resolution would require additional factors to be taken into account, such as photosensor dark current, transit time jitter, etc, but this is left for future publication. In this note we merely wish to illustrate that the different characteristics of SiPMs and PMTs make it interesting to compare the timing resolution achieved in this work with those published for PMTs in combination with the same scintillation material.

For example, a CRT of 240 ps FWHM has been measured with two, 4 mm × 4 mm × 30 mm $LaBr_3$:Ce(5%) crystals coupled to R4998 PMTs (Kuhn *et al* 2005), while Kyba *et al* (2008) reported a CRT of 160 ps FWHM for two ∅13 mm × 13 mm $LaBr_3$:Ce(5%) crystals coupled to the same PMTs, thereby demonstrating the dependence of CRT on crystal dimensions. A simulation by Kuhn *et al* (2005) predicts a CRT of ∼100 ps FWHM for very small crystals. The dependence of CRT on the time pick-off method was tested by Wiener *et al* (2008) by comparing analogue to digital methods. Although it was originally reported that the CRT with digital waveform sampling was superior, further work has since demonstrated that these measurements are sensitive to the assumptions made about the shape of the signal rising edge, and that the timing resolutions obtained with digital and analogue methods are comparable (private communication). Given these results, the present work indicates that SiPM-based scintillation detectors can provide timing resolutions at least as good as those obtained with PMTs.

It is noted that scintillators exist that may provide even better timing resolution than commercial-grade $LaBr_3$:Ce(5%). For example, increasing the Ce concentration in $LaBr_3$:Ce to ∼30% appears to improve timing resolution significantly (Glodo *et al* 2005, Kuhn *et al* 2005). Other materials, such as $CeBr_3$ and LuI_3:Ce, are also investigated as candidates for TOF-PET (Glodo *et al* 2006, Shah *et al* 2004, 2005). Hence, it would be interesting to study the timing performance of SiPMs in combination with $LaBr_3$:Ce(30%) and other promising new materials.

4.3. SiPM saturation

In principle, it might also be possible to further improve the timing resolution by using SiPMs containing fewer but larger microcells, thus improving their fill factor and, therefore, their PDE. However, if the number of microcells would be made too small, this might lead to excessive saturation. Such saturation causes the pulse height spectra of SiPM-based scintillation detectors to increasingly be compressed along the energy axis with increasing gamma energy (Buzhan *et al* 2001, Stoykov *et al* 2007). As can be seen from the relative positions of the 511 keV and 1275 keV peaks in figure 4, a significant degree of saturation already occurs in the present experiments. While the excellent energy resolution of $LaBr_3$:Ce already gives rise to a relatively small width of the 511 keV full-energy peaks, this implies that the peak widths observed in figure 4 are additionally reduced by SiPM saturation. From a practical point of view, however, it is important that well-resolved 511 keV full-energy peaks are still obtained. In a clinical PET system, this is crucial for accurate rejection of photons that have undergone Compton scattering in the patient.

It is noted that, in addition to SiPM saturation, the pulse height spectra may in principle also be influenced by electronic non-proportionality as described by Seifert *et al* (2008, 2009). However, this effect is expected to be small in our measurements.

5. Conclusions

The experiments presented here show that SiPM-based scintillation detectors for TOF-PET can provide timing resolutions at least as good as detectors based on conventional PMTs. At the

same time, pulse height spectra with well-resolved full-energy peaks can be obtained, which is necessary for accurate rejection of Compton-scattered photons. The use of $LaBr_3$:Ce(5%) allowed us to achieve a CRT of ∼100 ps FWHM for 511 keV annihilation photon pairs, corresponding to a TOF positioning resolution of ∼15 mm FWHM. To our knowledge this is the best experimental figure reported for SiPM-based scintillation detectors to date.

It is not unlikely that further optimization of scintillation materials and SiPM technology will lead to even better results in the near future. Given the advantages of SiPMs over PMTs, such as their small size, transparency to 511 keV gamma rays, magnetic field compatibility, etc, we conclude that detectors based on $LaBr_3$:Ce and SiPMs have high potential for use in TOF-PET devices.

Acknowledgments

We would like to thank Joel Karp of the Department of Radiology, University of Pennsylvania, PA, USA, for helpful discussions. This work was supported in part by SenterNovem under grant no IS055019.

References

Antich P P, Tsyganov E N, Malakhov N A and Sadygov Z Y 1997 Avalanche photo diode with local negative feedback sensitive to UV, blue and green light *Nucl. Instrum. Methods Phys. Res.* A **389** 491–8

Bizarri G and Dorenbos P 2007 Charge carrier and exciton dynamics in $LaBr_3:Ce^{3+}$ scintillators: experiment and model *Phys. Rev.* B **75** 184302–10

Bondarenko G *et al* 2000 Limited Geiger-mode microcell silicon photodiode: new results *Nucl. Instrum. Methods Phys. Res.* A **442** 187–92

Britvitch I, Johnson I, Renker D, Stoykov A and Lorenz E 2007 Characterization of Geiger-mode avalanche photodiodes for medical imaging applications *Nucl. Instrum. Methods Phys. Res.* A **571** 308–11

Burr K C and Wang G-C 2007 Scintillation detection using 3 mm× 3 mm silicon photomultipliers *2007 IEEE Nucl. Sci. Symp. Conf. Record* pp 975–82

Buzhan P *et al* 2001 An advanced study of silicon photomultiplier *ICFA Instrum. Bull.* **23** 28–42

Catana C, Wu Y, Judenhofer M S, Qi J, Pichler B J and Cherry S R 2006 Simultaneous acquisition of multislice PET and MR images: initial results with a MR-compatible PET scanner *J. Nucl. Med.* **47** 1968–76

Daube-Witherspoon M E, Surti S, Perkins A, Kyba C C M, Wiener R, Werner M E, Kulp R and Karp J S 2010 The imaging performance of a $LaBr_3$-based PET scanner *Phys. Med. Biol.* **55** 45–64

de Haas J T M and Dorenbos P 2008 Advances in yield calibration of scintillators *IEEE Trans. Nucl. Sci.* **55** 1086–92

Drozdowski W, Dorenbos P, Bos A J J, de Haas J T M, Kraft S, Maddox E, Owens A, Quarati F G A, Dathy C and Ouspenski V 2007 Effect of proton dose, crystal size, and cerium concentration on scintillation yield and energy resolution of $LaBr_3$:Ce *IEEE Trans. Nucl. Sci.* **54** 736–40

Du Y and Retière F 2008 After-pulsing and cross-talk in multi-pixel photon counters *Nucl. Instrum. Methods Phys. Res.* A **596** 396–401

España S, Fraile L M, Herraiz J L, Udias J, Desco M and Vaquero J J 2010 Performance evaluation of SiPM photodetectors for PET imaging in the presence of magnetic fields *Nucl. Instr. Methods Phys. Res.* A **613** 308–16

Glodo J, Kuhn A, Higgins W M, Van Loef E V D, Karp J S, Moses W W, Derenzo S E and Shah K S 2006 $CeBr_3$ for time-of-flight PET 2006 *IEEE Nucl. Sci. Symp. Conf. Record* pp 1570–3

Glodo J, Moses W W, Higgins W M, van Loef E V D, Wong P, Derenzo S E, Weber M J and Shah K S 2005 Effects of Ce concentration on scintillation properties of $LaBr_3$:Ce *IEEE Trans. Nucl. Sci.* **55** 1805–8

Golovin V and Saveliev V 2004 Novel type of avalanche photodetector with Geiger mode operation *Nucl. Instrum. Methods Phys. Res.* A **518** 560–4

Gottlich M, Garutti E, Kozlov V, Schultz-Coulon H-C, Tadday A and Terkulov A 2008 Application of multi-pixel photon counter to positron emission tomography *2008 IEEE Nucl. Sci. Symp. Conf. Record* pp 3119–22

Hamamatsu Corporation 1999 Photomultiplier tube R4998 TPMH1261E02 December 1999 (Hamamatsu Photonics K K) http://www.hamamatsu.com

Hamamatsu Corporation 2009 MPPC (multi-pixel photocounter) S10362 series, S10931 series Cat. No. KAPD1023E03 July 2009 DN (Hamamatsu Photonics K K) http://www.hamamatsu.com

Herbert D J, Moehrs S, D'Ascenzo N, Belcari N, Del Guerra A, Morsani F and Saveliev V 2007 The silicon photomultiplier for application to high-resolution positron emission tomography *Nucl. Instrum. Methods Phys. Res.* A **573** 84–7

Higgins W M, Glodo J, van Loef E, Klugerman M, Gupta T, Cirignano L, Wong P and Shah K S 2006 Bridgman growth of $LaBr_3$:Ce and $LaCl_3$:Ce crystals for high-resolution gamma-ray spectrometers *J. Cryst. Growth* **287** 239–42

Judenhofer M S *et al* 2008 Simultaneous PET-MRI: a new approach for functional and morphological imaging *Nat. Med.* **14** 459–65

Kadrmas D J, Casey M E, Conti M, Jakoby B W, Lois C and Townsend D W 2009 Impact of time-of-flight on PET tumor detection *J. Nucl. Med.* **50** 1315–23

Kim C L, Wang G C and Dolinsky S 2009 Multi-pixel photon counters for TOF PET detector and its challenges *IEEE Trans. Nucl. Sci.* **56** 2580–5

Kolb A, Judenhofer M S, Lorenz E, Renker D and Pichler B J 2008 PET block detector readout approaches using G-APDs *2008 IEEE Nucl. Sci. Symp. Conf. Record*

Kuhn A, Surti S, Karp J S, Muehllehner G, Newcomer F M and VanBerg R 2006 Performance assessment of pixelated $LaBr_3$ detector modules for time-of-flight PET *IEEE Trans. Nucl. Sci.* **53** 1090–5

Kuhn A, Surti S, Shah K S and Karp J S 2005 Investigation of $LaBr_3$ detector timing resolution 2005 *IEEE Nucl. Sci. Symp. Conf. Record* pp 2022–6

Kyba C C M, Glodo J, van Loef E V D, Karp J S and Shah K S 2008 Energy and timing response of six prototype scintillators for TOF-PET *IEEE Trans. Nucl. Sci.* **55** 1404–8

Lewellen T K 2008 Recent developments in PET detector technology *Phys. Med. Biol.* **53** R287–317

Llosá G *et al* 2008 Evaluation of the first silicon photomultiplier matrices for a small animal PET scanner *2008 IEEE Nucl. Sci. Symp. Conf. Record* pp 3574–80

Lois C, Jakoby B W, Long M J, Hubner K F, Barker D W, Casey M E, Conti M, Panin V Y, Kadrmas D J and Townsend D W 2010 An assessment of the impact of incorparating time-of-flight information into clinical PET/CT imaging *J. Nucl. Med.* **51** 237–45

McElroy D P, Saveliev V, Reznik A and Rowlands L A 2007 Evaluation of silicon photomultipliers: a promising new detector for MR compatible PET *Nucl. Instrum. Methods Phys. Res.* A **571** 106–9

Moses W W 2007 Recent advances and future advances in time-of-flight PET *Nucl. Instrum. Methods Phys. Res.* A **580** 919–24

Moses W W and Derenzo S E 1999 Prospects for time-of-flight PET using LSO scintillator *IEEE Trans. Nucl. Sci.* **46** 474–8

Muehllehner G and Karp J S 2006 Positron emission tomography *Phys. Med. Biol.* **51** R117-37

Musienko Y, Auffray E, Lecoq P, Reucroft S, Swain J and Trummer J 2007 Study of multi-pixel Geiger-mode avalanche photodiodes as a read-out for PET *Nucl. Instrum. Methods Phys. Res.* A **571** 362–5

Nishikido F, Inadama N, Shibuya K, Yoshida E, Yamaya T, Oda I, Kitamura K and Murayama H 2008 Four-layer DOI-PET detector with a silicon photomultiplier array *2008 IEEE Nucl. Sci. Symp. Conf. Record* pp 3923–5

Pestotnik R, Korpar S, Chagani H, Dolenec R, Krizan P and Stanovnik A 2008 Silicon photo-multipliers as photon detectors for PET *2008 IEEE Nucl. Sci. Symp. Conf. Record* pp 3123–7

Renker D 2007 New trends in photodetectors *Nucl. Instrum. Methods Phys. Res.* A **71** 1–6

Schaart D R, Seifert S, van Dam H T, de Boer M R, Vinke R, Dendooven P, Löhner H and Beekman F J 2008a First experiments with $LaBr_3$:Ce crystals coupled directly to silicon photomultipliers for PET applications *2008 IEEE Nucl. Sci. Symp. Conf. Record* pp 3991–4

Schaart D R, van Dam H T, Seifert S, Vinke R, Dendooven P, Löhner H and Beekman F J 2008b SiPM-array based PET detectors with depth-of-interaction correction *2008 IEEE Nucl. Sci. Symp. Conf. Record* pp 3581–5

Schaart D R, van Dam H T, Seifert S, Vinke R, Dendooven P, Löhner H and Beekman F J 2009 A novel, SiPM-array-based, monolithic scintillator detector for PET *Phys. Med. Biol.* **54** 3501–12

Seifert S, Schaart D R, van Dam H T, Huizenga J, Vinke R, Dendooven P, Löhner H and Beekman F J 2008 A high bandwidth preamplifier for SiPM-based TOF PET scintillation detectors *2008 IEEE Nucl. Sci. Symp. Conf. Record* pp 1616–9

Seifert S, van Dam H T, Huizenga J, Vinke R, Dendooven P, Löhner H and Schaart D R 2009 Simulation of silicon photomultiplier signals *IEEE Trans. Nucl. Sci.* **56** 3726–33

Shah K S, Glodo J, Higgins W, van Loef E V D, Moses W W, Derenzo S E and Weber M J 2005 $CeBr_3$ scintillators for gamma-ray spectroscopy *IEEE Trans. Nucl. Sci.* **52** 3157–9

Shah K S, Glodo J, Klugerman M, Higgins W, Gupta T, Wong P, Moses W W, Derenzo S E, Weber M J and Dorenbos P 2004 LuI_3:Ce—a new scintillator for gamma ray spectroscopy *IEEE Trans. Nucl. Sci.* **51** 2302–5

Shao Y, Cherry S R, Farahani K, Slates R, Silverman R W, Meadors K, Bowery A, Siegel S, Marsden P K and Garlick P B 1997 Development of a PET detector system compatible with MRI/NMR systems *IEEE Trans. Nucl. Sci.* **44** 1167–71

Shibuya K, Nishikido F, Tsuda T, Kobayashi T, Lam C, Yamaya T, Yoshida E, Inadama N and Murayama H 2008 Timing resolution improvement using DOI information in a four-layer scintillation detector for TOF-PET *Nucl. Instrum. Methods Phys. Res.* A **593** 572–7

Song T Y, Wu H, Komarov S, Siegel S B and Tai Y-C 2008 Sub-millimeter resolution PET detector module using multi-pixel photon counter array *2008 IEEE Nucl. Sci. Symp. Conf. Record* pp 4933–7

Stoykov A, Musienko Y, Kuznetsov A, Reucroft S and Swain J 2007 On the limited amplitude resolution of multipixel Geiger-mode APDs *J. Instrum.* **2** P06005

Surti S, Kuhn A, Werner M E, Perkins A E, Kolthammer J and Karp J S 2007 Performance of Philips Gemini TF PET/CT scanner with special consideration for its time-of-flight imaging capabilities *J. Nucl. Med.* **48** 471–80

Townsend D W 2008 Multimodality imaging of structure and function *Phys. Med. Biol.* **53** R1–R39

van Eijk C W E 2002 Inorganic scintillators in medical imaging *Phys. Med. Biol.* **47** R85–R106

Vinke R, Löhner H, Schaart D R, van Dam H T, Seifert S, Beekman F B and Dendooven P 2008 Optimizing timing resolution for TOF PET detectors based on monolithic scintillation crystals using fast photosensor arrays *2008 IEEE Nucl. Sci. Symp. Conf. Record* pp 3954–60

Wiener R I, Surti S, Kyba C C M, Newcomer F M, Van Berg R and Karp J S 2008 An investigation of waveform sampling for improved signal processing in TOF PET *2008 IEEE Nucl. Sci. Symp. Conf. Record* pp 4101–5

Wilmshurst T H 1985 *Signal Recovery from Noise in Electronic Instrumentation* (Bristol: Hilger)

Yamamoto K, Yamamura K, Sato K, Ota T, Suzuki H and Ohsuka S 2007 Development of multi-pixel photon counter (MPPC) *2007 IEEE Nucl. Sci. Symp. Conf. Record* pp 1094–7